Supporting Information

Single Photon Emission from Plasma Treated 2D Hexagonal Boron Nitride

Zai-Quan Xu[1], Christopher Elbadawi[1], Toan Trong Tran[1], Mehran Kianinia[1], Xiuling Li[2], Daobin Liu[2 3], Timothy B. Hoffman[4], Minh Nguyen[1], Sejeong Kim[1], James H. Edgar[4], Xiaojun Wu[2], Li Song[2 3], Sajid Ali[1], Mike Ford[1], Milos Toth[1]** and *Igor Aharonovich[1]**

[1] School of Mathematical and Physical Sciences, Faculty of Science, University of Technology Sydney, Ultimo, 2007, New South Wales, Australia

[2] School of Chemistry and Materials Sciences, CAS Key Lab of Materials for Energy Conversion, and CAS Center for Excellence in Nanoscience, Hefei National Laboratory of Physics at the Microscale, Synergetic Innovation of Quantum Information & Quantum Technology, University of Science and Technology of China, Hefei, Anhui 230026, China

[3] National Synchrotron Radiation Laboratory, CAS Center for Excellence in Nanoscience, University of Science and Technology of China, Hefei, Anhui 230029, China.

[4]Department of Chemical Engineering, Durland Hall, Kansas State University, Manhattan, KS 66506, USA

Corresponding Emails: Zaiquan.xu@uts.edu.au; Milos.Toth@uts.edu.au; Igor.Aharonovich@uts.edu.au

Keywords: two-dimensional materials, hexagonal-boron nitride, single photon emitters, plasma etching, oxygen doped atomic defects

Figure S1 shows examples of the stability curves of the emitters that formed after plasma processing and undergone the 2nd annealing step.

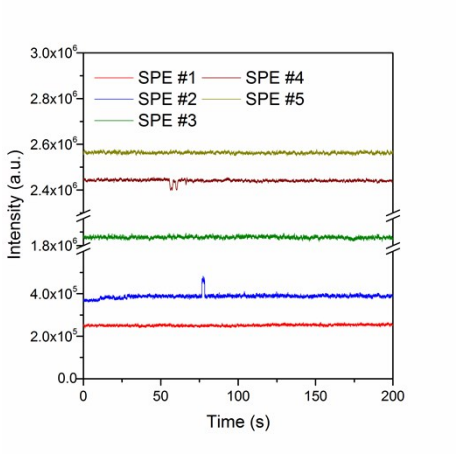

Figure S1 Stability curves (photon counts per second as a function of time) from four different emitters found in hBN crystals after plasma and annealing.

In order to leverage the observation that emitters are generated preferentially at edges, we explored the possibility of using photolithography to localize emitters by creating annuli that were subsequently processed by the Ar plasma treatment. Figure S2a shows an optical microscope image of the hBN crystal. The outer diameter of each annulus is ~2 μm and the center-to-center distance is 4 μm. We intentionally chose a relatively large hBN flake in order to fit an array of ~ 9 annuli on a single crystal. Figure S2b shows a confocal PL image of the crystal, revealing the presence of a number of localized bright regions. The red circles highlight the positions of 5 emitters found in this sample, all of which were found to be in the vicinity of the annuli (within the confocal microscope resolution of ~ 400 nm). Figure S2c shows PL spectra collected from these spots, demonstrating that they are narrowband emitters with ZPL energies in the range of 580 to 680 nm, consistent with the results in Figure 1. Although the emitters are mostly on the created annuli, coincidentally, they are also in close vicinity of grain boundaries.

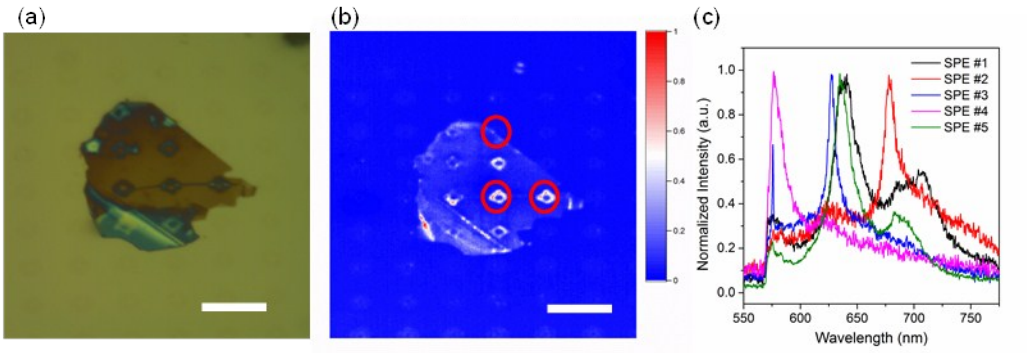

Figure S2 (a) Optical microscope image of annuli fabricated on a hBN crystal by plasma etching. Scale bar: 8 μm. (b) Normalized confocal PL map taken using a 580 nm long pass filer. (c) Selected PL spectra of emitters found in this crystal.

Oxygen plasma etching was investigated as an alternative to the Ar plasma etch treatment. It causes the fluorescence intensity of as-prepared hBN crystals to increase substantially, which may be caused in part by the generation of boron oxides in the samples. The O_2 plasma increases the concentration of emitters in the samples, but they exhibit severe blinking and eventual photobleaching during analysis, even in samples that were annealed in Ar using the conditions that stabilize emitters generated by the above Ar plasma treatment.

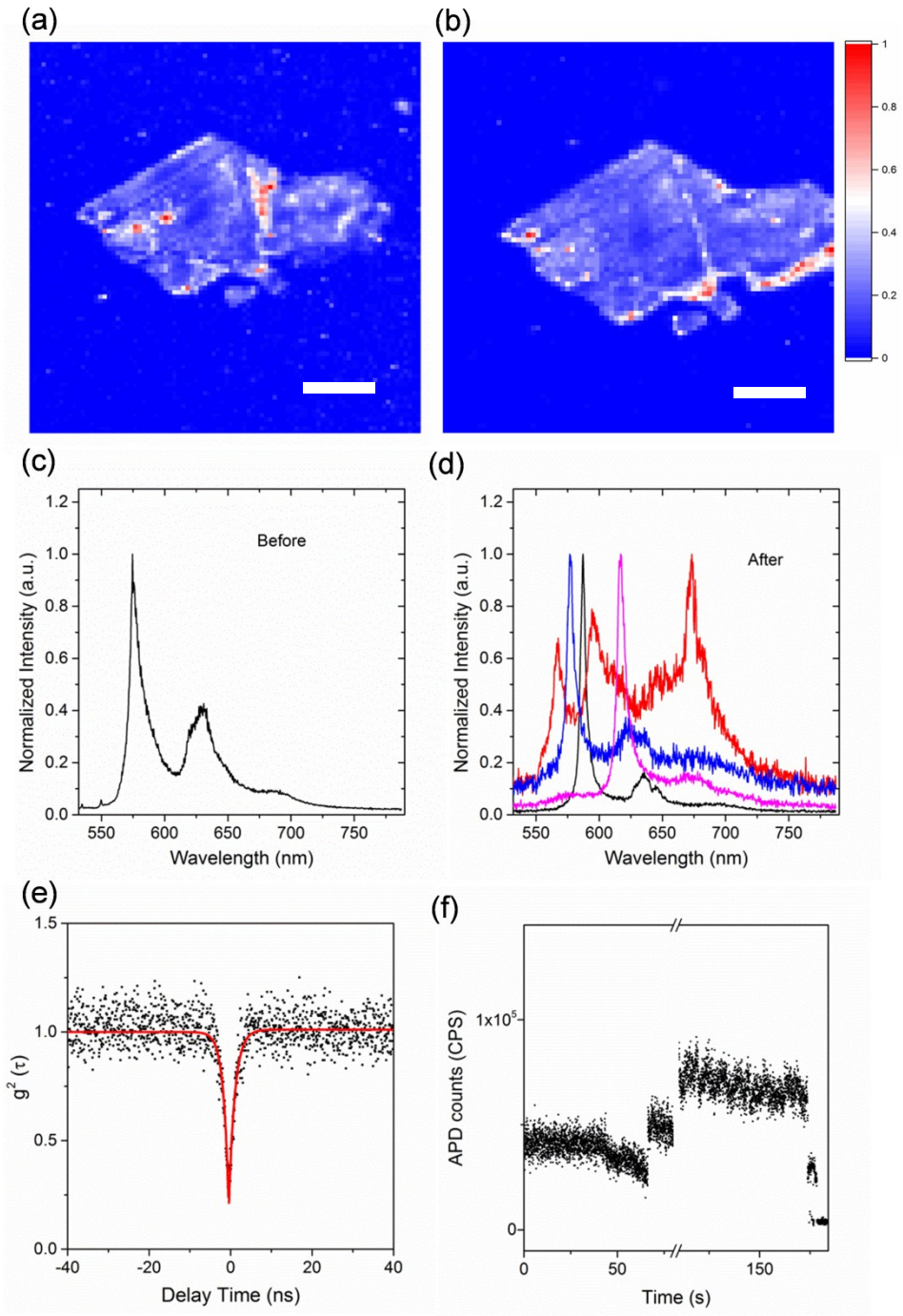

Figure S3 Confocal PL mapping over the same hBN flake before (a) and after (b) oxygen plasma etching. Scale bar: 8 μm. PL spectra of a single photon emitter found before (c) and after (d) O_2 plasma etching on the same hBN crystal. (e) Auto second correlation function of a single photon emitter created by O_2 plasma. (f) A typical APD counts as a function of time shows the poor stability of the new emitters produced from O_2 plasma.

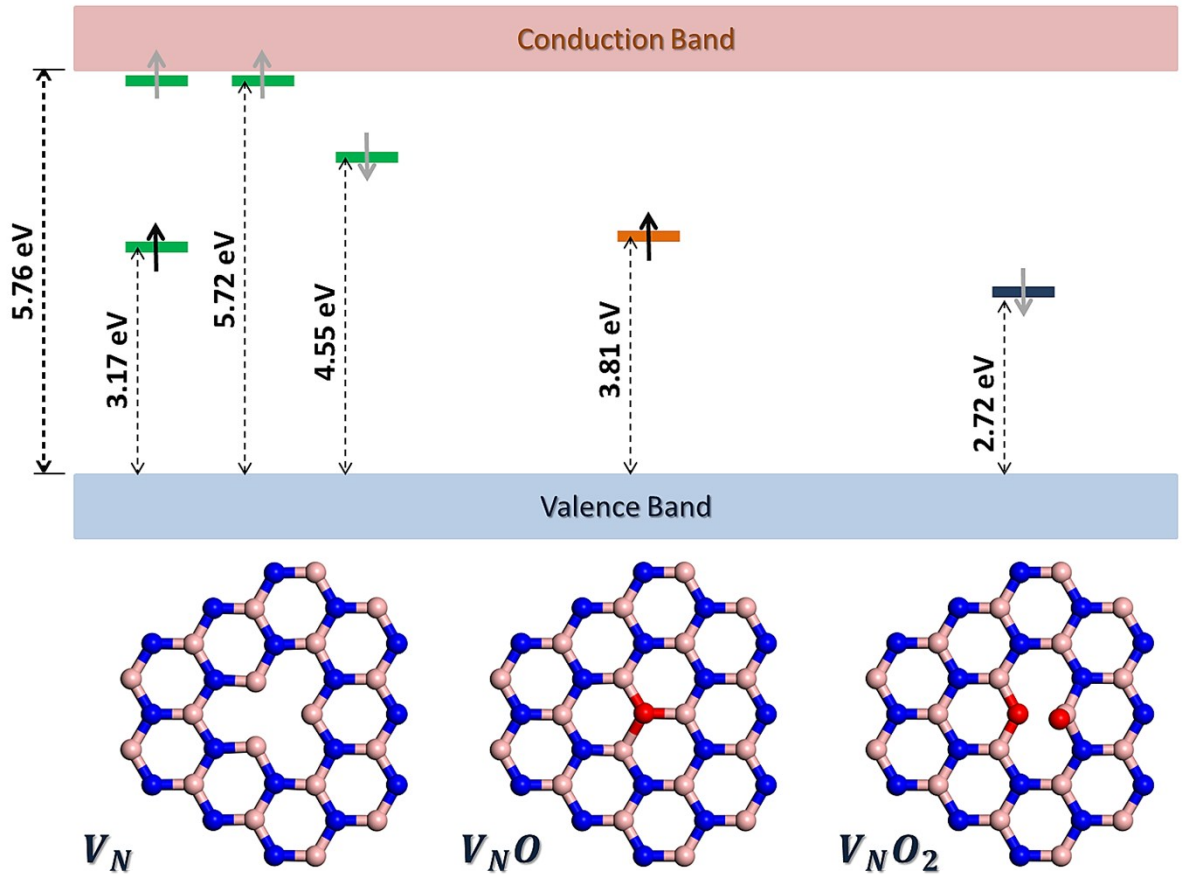

Figure S4. Schematics and simulated electronic structures for *N*-vacancy (^{V_N}), *N*-vacancy with one oxygen atom doping (^{V_NO}), and *N*-vacancy with two oxygen atoms doping (^{V_NO_2}). Black and grey arrows denote the occupied and unoccupied impurity states, respectively. Up and down arrows describe different spin.

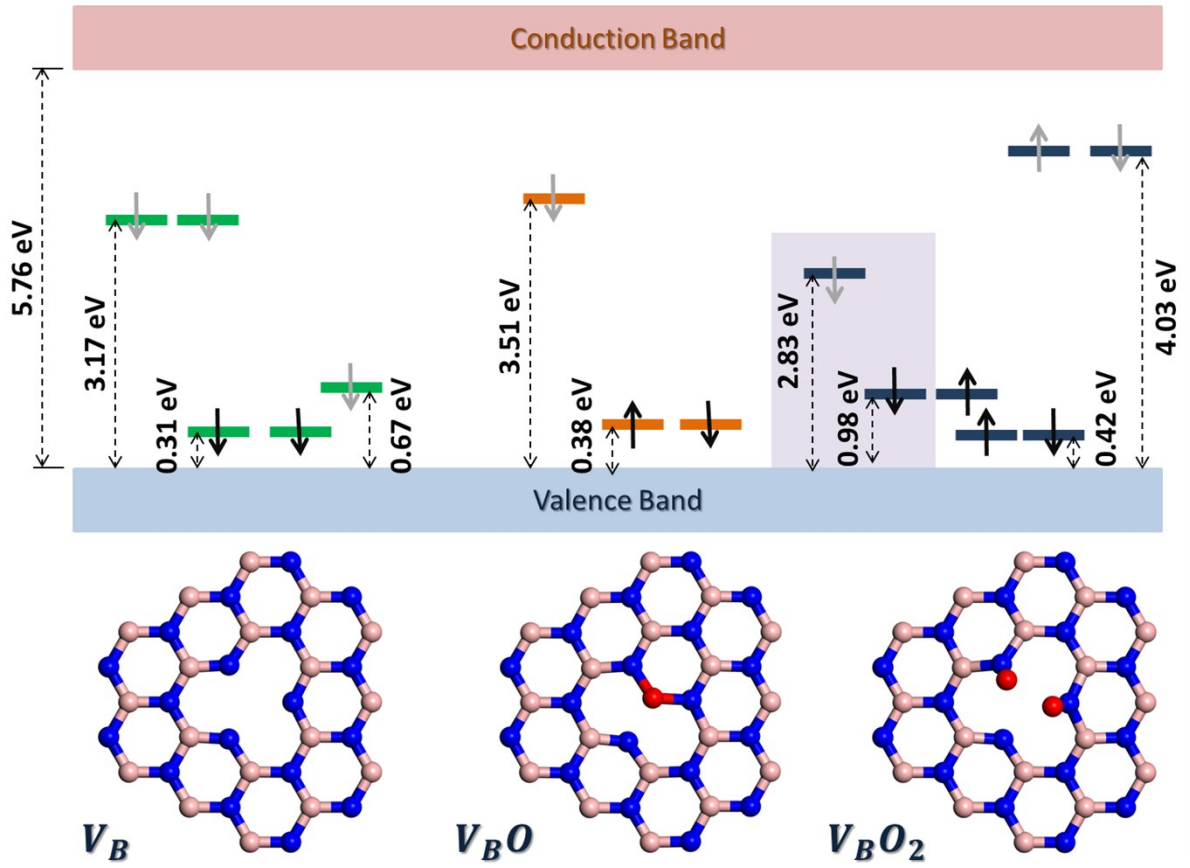

Figure S5. Schematics and simulated electronic structures for *B*-vacancy (^{V_B}), *B*-vacancy with one oxygen atom doping (^{V_BO}), and *B*-vacancy with two oxygen atoms doping (^{V_BO_2}). Black and grey arrows denote the occupied and unoccupied impurity states, respectively. Up and down arrows describe different spin.

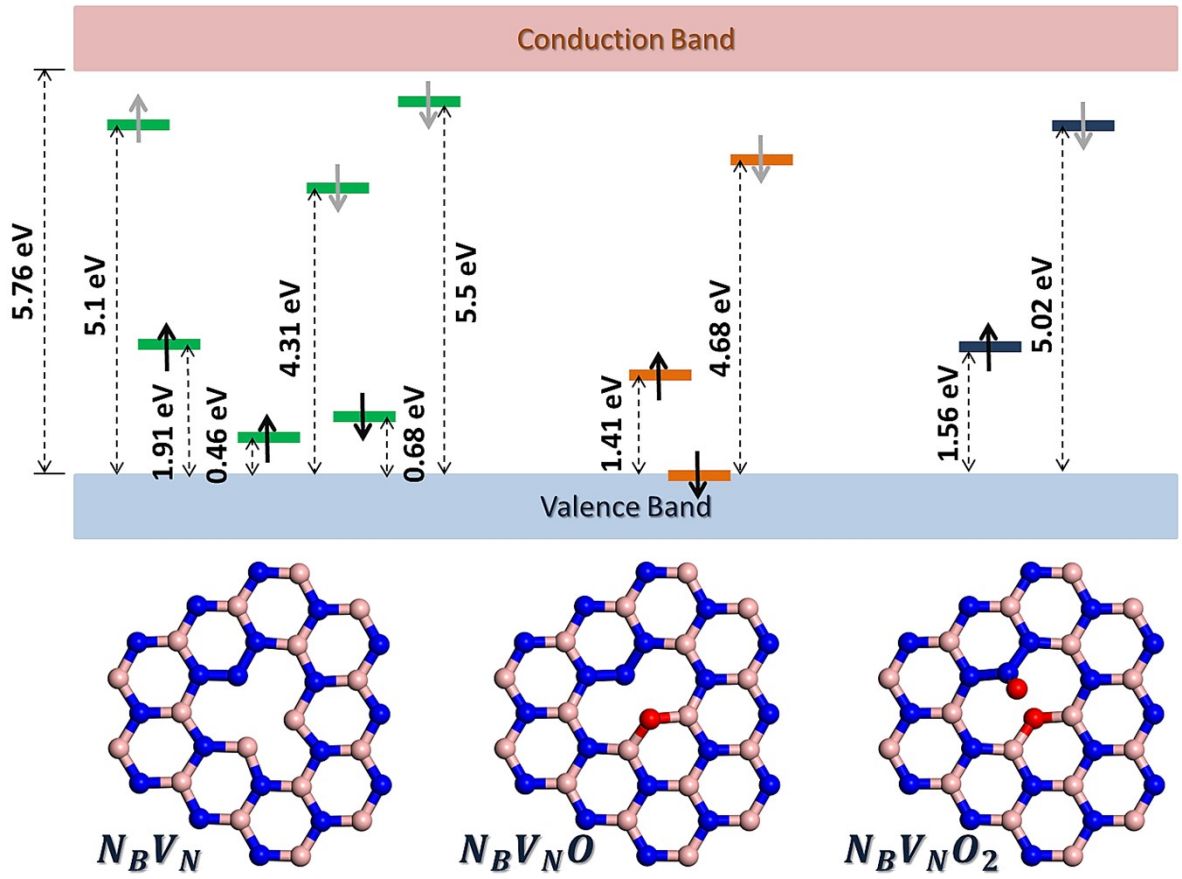

Figure S6. Schematics and simulated electronic structures for anti-site vacancy (^{N_BV_N}), anti-site vacancy with one oxygen atom doping (^{N_BV_NO}), and anti-site vacancy with two oxygen atoms doping (^{N_BV_NO_2}). Black and grey arrows denote the occupied and unoccupied impurity states, respectively. Up and down arrows describe different spin.